Reconstruction of solar spectral resource using limited spectral sampling for concentrating photovoltaic systems

Viktar Tatsiankou*[a], Karin Hinzer[a], Jafaru Mohammed[a], Aaron Muron[a], Matthew Wilkins[a], Joan Haysom[a], Henry Schriemer[a], and Stefan Myrskog[b]

[a]SUNLAB, University of Ottawa, 800 King Edward Ave., Ottawa, ON, Canada K1N 8P5;
[b]Morgan Solar Inc., 30 Ordnance St., Toronto, ON, Canada M6K 1A2

ABSTRACT

One of the challenges associated with forecasting and evaluating concentrating photovoltaic system (CPV) performance in diverse locations is the lack of high-quality spectral solar resource data. Various local atmospheric conditions such as air mass, aerosols, and atmospheric gases affect daily CPV module operation. A multi-channel filter radiometer (MFCR) can be used to quantify these effects at relatively low cost. The proposed method of selectively sampling the solar spectrum at specific wavelength channels to spectrally reconstruct incident irradiance is described and extensively analyzed. Field spectroradiometer (FSR) measurements at the University of Ottawa's CPV testing facility (45.42°N, 75.68°W) are fed into our model to mimic the outputs from the MCFR. The analysis is performed over a two year period (2011–2012), using 46,564 spectra. A recommendation is made to use four aerosols channels at 420, 500, 780, and 1050 nm, one ozone channel at 610 nm and one water vapour channel at 940 nm, all of which can be measured with ubiquitous Si photodiodes. A simulation of this MFCR channel configuration produces an RMS error under 1.5% over 96% of the 350–1830 nm range, when compared with the FSR, for the 2012 data set in Ottawa.

Keywords: solar spectrum, modelling, photovoltaics, spectroradiometer, multi-channel filter radiometer

1. INTRODUCTION

The solar irradiance at ground level is a dynamic energy resource that fluctuates in intensity and spectrum due to varying geographical and meteorological conditions. Air mass (AM), aerosols, atmospheric gases (oxygen, ozone, water vapour, etc.), and numerous pollutants act in conjunction as a continuously varying filter of extraterrestrial solar irradiance (AM0). Photovoltaic (PV) solar cells are sensitive to such spectral fluctuations, as demonstrated by numerous experimental and theoretical studies[1–10]. However, different solar cell technologies exhibit varying degrees of sensitivity to spectral changes in illumination. Multi-junction solar cells (MJSC), which are at heart of the most concentrating photovoltaic systems (CPV), are more sensitive to direct normal spectral irradiance (spectral DNI) variation than their silicon solar cell counterparts. This is due to the fact that MJSC are series connected, which results in the worst performing sub-cell limiting the performance of the full device. Furthermore, future MJSC designs are expected to incorporate up to six junctions, which makes them even more sensitive to incident solar spectrum variation[11]. As a result, MJSC sub-cells are designed to be current matched for a particular spectrum, such as for the AM1.5D reference ASTM G173[12–14]. Under realistic conditions spectral variations cause MJSC and consequently CPV system performance to deviate from the desired operating point. Therefore, knowledge of the spectral distribution of the solar resource at a particular installation site is a valuable asset that can give a better predictive insight into the operation of the CPV system.

At present, the most accurate way to obtain solar spectra at a desired location is to perform direct outdoor measurements with a field spectroradiometer (FSR). However, these measurements are rarely available due to the prohibitive cost of the instrument. An alternative approach is to use modelling tools in conjunction with available local meteorological inputs, such as atmospheric pressure, ambient temperature and humidity, to produce an approximated spectrum. The most common way to simulate spectral DNI is through the use of the Simple Model of the Atmospheric Radiative Transfer of Sunshine (SMARTS2), which has become the de-facto

Photonics North 2013, Pavel Cheben, Jens Schmid, Caroline Boudoux, Lawrence R. Chen, André Delâge, Siegfried Janz, Raman Kashyap, David J. Lockwood, Hans-Peter Loock, Zetian Mi, Eds., Proc. of SPIE Vol. 8915, 891506 · © 2013 SPIE · CCC code: 0277-786X/13/$18 · doi: 10.1117/12.2033613

standard in the solar community[15,16]. However, to do so accurately, SMARTS2 requires inputs such as aerosol optical depth at 500 nm, water vapour content, and ozone column amount, which are not typically available locally. Aerosol Robotic Network (AERONET) sites can be used to determine the aforementioned parameters if a nearby site is available (600 sites are currently in operation worldwide)[17,18]. However, a leading option is to interpolate AERONET data for the desired location using measurements from nearby sites[2].

In this paper, a method of limited spectral sampling is analyzed by using a simulated multi-channel filter radiometer (MCFR) to reconstruct incident local solar spectra. An MCFR is an instrument that measures solar irradiance in several narrow wavelength bands with a combination of interference filters and photodiodes. This device can perform spectral measurements at a fraction of the cost of a spectroradiometer[19], but additional post-processing is required to deduce the solar spectrum. Therefore, it is of interest to quantify the accuracy of the MCFR for inferring spectral irradiance as the number and type of channels is varied.

2. METHODOLOGY

2.1. Calculation of spectral direct normal irradiance

On a clear, cloudless day the spectral DNI can be written as

$$S(\lambda) = S_0(\lambda) \cdot r^2 \cdot T_{\mathrm{a}}(\lambda) \cdot T_{\mathrm{g}}(\lambda) \cdot T_{\mathrm{n}}(\lambda) \cdot T_{\mathrm{o}}(\lambda) \cdot T_{\mathrm{R}}(\lambda) \cdot T_{\mathrm{w}}(\lambda), \tag{1}$$

where $S_0(\lambda)$ is the extraterrestrial irradiance (or AM0), r is the ratio of the average to actual Sun to Earth distance, and T_{i} is the transmittance of the atmospheric constituent, with the subscripts "a", "g", "n", "o", "R", and "w" referring to aerosol absorption and scattering, mixed gas absorption (O_2, CO_2, and CH_4), NO_2 absorption, ozone absorption, Rayleigh scattering, and water vapour absorption, respectively. The AM0 spectrum, with an integrated irradiance value of 1366.1 W/m^2, is adapted from the most recent measurements and analysis[?] .

Equation (1) can be expressed equivalently with Beer's law as

$$S(\lambda) = S_0(\lambda) \cdot r^2 \cdot \exp\big[-\big(\tau_{\mathrm{a}}(\lambda) \cdot m_{\mathrm{a}} + \tau_{\mathrm{g}}(\lambda) \cdot m_{\mathrm{g}} + \tau_{\mathrm{n}}(\lambda) \cdot m_{\mathrm{n}} + \tau_{\mathrm{o}}(\lambda) \cdot m_{\mathrm{o}} + \tau_{\mathrm{R}}(\lambda) \cdot m_{\mathrm{R}} + \tau_{\mathrm{w}}(\lambda) \cdot m_{\mathrm{w}}^*\big)\big], \tag{2}$$

where τ_i and m_i are the optical depth and the AM associated with each atmospheric component. The optical depth is a dimensionless measure of atmospheric transparency, as influenced by absorption and scattering. The AM values are functions of the zenith angle of the sun. The general expression for the AM of each component can be written as[16]

$$m_i = \big[\cos(Z) + \kappa_{i1} \cdot Z^{\kappa_{i2}} \cdot (\kappa_{i3} - Z)^{\kappa_{i4}}\big]^{-1}, \tag{3}$$

where Z is the zenith angle (°) of the sun, calculated with the National Renewable Energy Laboratory (NREL) solar position algorithm within uncertainties of $\pm 0.0003^{\circ}$[20]. The κ_{ij} parameters are given in Table 1[21].

Table 1. Optical air mass coefficients for equation 3.

Optical airmass	i	κ_{i1}	κ_{i2}	κ_{i3}	κ_{i4}
Aerosols (m_{a})	1	0.169	0.182	95.318	-1.954
Mixed gases (m_{g})	2	0.484	0.0959	96.741	-1.754
Nitrogen dioxide (m_{n})	3	1.121	1.613	111.55	-3.263
Ozone (m_{o})	4	1.065	0.638	101.8	-2.269
Rayleigh (m_{R})	5	0.484	0.0959	96.741	-1.754
Water vapour (m_{w}^*)	6	0.107	0.114	93.781	-1.920

Note: $m_{\mathrm{w}}^* = m_{\mathrm{w}}^{0.943}$

Aerosol extinction can be modelled empirically with Ångström's power law[22] as

$$\tau_{\mathrm{a}}(\lambda) = \beta_{\mathrm{y}} \cdot \lambda^{-\alpha_{\mathrm{y}}}, \tag{4}$$

where β_y and α_y are coefficients that are determined experimentally. Aerosol extinction is divided into y regions over the FSR's measured 350–1830 nm range, where $y+1$ is the number of aerosol dedicated channels. For example, for the MCFR with four aerosol channels, three sets of β_y and α_y coefficients are calculated and applied to the corresponding spectral region y for all wavelengths between two adjacent aerosol channels.

Optical depth due to mixed gases is caused by the cumulative effect of multiple gases that are uniformly distributed in the atmosphere and is represented by total column abundances of each gas, which are additive. Only the constituents that significantly affect the results in the FSR's measured 350–1830 nm range are selected in the simulations. Consequently, the mixed gases optical depth can be expressed as

$$\tau_g(\lambda) = p_{CH_4} \cdot A_{CH_4}(\lambda) + p_{CO_2} \cdot A_{CO_2}(\lambda) + p_{O_2} \cdot A_{O_2}(\lambda), \tag{5}$$

where p_i is the path length (or the total column abundance) of the constituent gas (in atm-cm) and $A_i(\lambda)$ is its wavelength-dependent absorption coefficient (in cm^{-1}). The total column abundance of a constituent gas is affected by changes in temperature and pressure. Its general expression is written as[21]

$$p_i = \chi_g \cdot H \cdot P_r^{\gamma} \cdot T_r^{\varphi}, \tag{6}$$

where is χ_g the volume mixing ratio of gas (in ppmv), $H = 8.429 \times 10^5$ cm, is the scale height of the isothermal atmosphere with T=288 K at sea-level pressure, P_r and T_r are ratios of actual to reference pressure and temperature respectively, and γ, φ are pressure and temperature correction coefficients, respectively. Table 2 presents assumed volume mixing ratios of mixed gases along with pressure and temperature correction coefficients.

Table 2. Mixed gases volume mixing ratios[23] with pressure and temperature correction coefficients[21].

Mixed gas	χ_g(ppmv)	γ	φ
Methane (CH_4)	1.8	1.125	0.0473
Carbon dioxide (CO_2)	375	1	0
Oxygen (O_2)	209500	1	0

Ozone optical depth can be expressed as

$$\tau_o(\lambda) = p_o \cdot A_o(\lambda) \cdot C_o(\lambda), \tag{7}$$

where $A_o(\lambda)$ is its absorption coefficient in (cm^{-1}), $C_o(\lambda)$ is a unitless ozone temperature correction function and p_o is the experimentally determined ozone path length (in atm-cm).

Nitrogen dioxide's optical depth $\tau_n(\lambda)$ is a highly variable atmospheric quantity, deriving from both natural and anthropogenic sources. Its expression is the same as (7) utilizing an absorption coefficient $A_n(\lambda)$ and a temperature correction function $C_n(\lambda)$. A total column abundance $p_n = 0.00118$ atm-cm is used, which is the average concentration of nitrogen dioxide in Montreal, Canada in 2005 with the assumption that this pollution layer is 1 km thick[24].

Rayleigh scattering is a well-understood phenomenon[25,26]. A least-squares fit is used to determine the optical depth as[21]

$$\tau_R(\lambda) = \frac{P_r}{\beta_1 \cdot \lambda^4 + \beta_2 \cdot \lambda^2 + \beta_3 + \beta_4 \cdot \lambda^{-2}}, \tag{8}$$

where P_r is the ratio of site to sea level ambient pressure, $\beta_1 = 117.341$ nm^{-4}, $\beta_2 = 1.511$ nm^{-2}, $\beta_3 = 0.0175$, and $\beta_4 = 8.774$ nm^2.

An expression for precipitable water vapour is formulated as[21]

$$\tau_w(\lambda) = p_w^{0.943} \cdot \varepsilon_1(\lambda) \cdot \varepsilon_2(\lambda) \cdot A_w(\lambda), \tag{9}$$

where $A_w(\lambda)$ is its wavelength-dependent absorption coefficient (cm^{-1}), $\varepsilon_1(\lambda)$ is the pressure scaling factor that accounts for water vapour's inhomogeneity in the atmosphere, $\varepsilon_1(\lambda)$ is the correction factor that improves parameterization away from the band center under fluctuating humidity conditions, and p_w is experimentally determined water vapour path length (in atm-cm). Absorption coefficients and correction factors for all atmospheric constituents are used with minor modifications from SMARTS2 unless otherwise indicated[15,16].

2.2. Simulation of multi-channel filter radiometer

Based on the number of desired channels and filter characteristics the corresponding Gaussian filter's transmittance profiles are generated and applied to measured solar spectra as shown in Figure 1. Spectral current density is determined from the responsivity of the photodiode (typically Si or Ge), as demonstrated in Figure 2. Integration of the spectral current density over all wavelengths gives the current density for each channel. Finally, the measured photodiode current, $I_{x,\text{measured}}$, for each channel x can be expressed as

$$I_{x,\text{measured}} = A \cdot \int_{\lambda_1}^{\lambda_2} S(\lambda) \cdot F_x(\lambda) \cdot R(\lambda) \cdot d\lambda, \tag{10}$$

where A is the active area of the photodiode, $S(\lambda)$ is the measured spectrum, $F_x(\lambda)$ is the filter transmittance of channel x, $R(\lambda)$ is the responsivity of the photodiode, and λ_1, λ_2 is the wavelength range of the channel. Since the full widths at half maxima (FWHM) of the MCFR's filters are narrow, typically 1-10 nm[19], the integration is not performed for the entire spectral range. It is assumed that the filters have no out-of-band transmittance. Hence, inputs into the model are x values representing current measured from each channel.

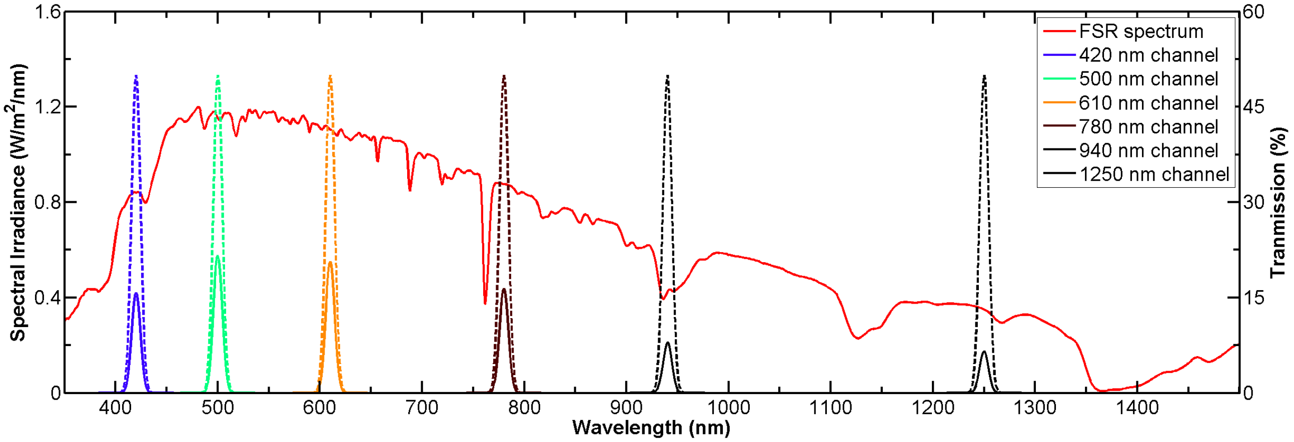

Figure 1. Dashed lines are Gaussian filter transmittance profiles for each channel of the MCFR. The corresponding solid lines are the product of filter transmittance and a sample solar spectrum (red line).

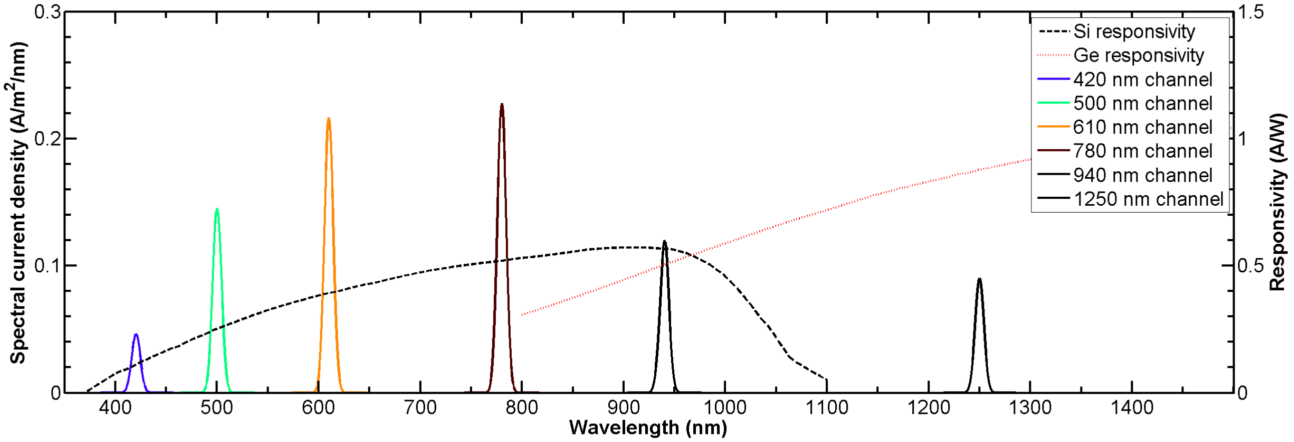

Figure 2. Application of photodiode responsivity to each channel of the MCFR.

2.3. Channel selection for parameterization

Aerosol extinction affects all wavelengths of the solar spectrum in the 350–1830 nm range, but ozone and water vapour absorption are only significant in discrete spectral regions. Figure 3 shows the transmittance of ozone and water vapour as their total column abundances are varied from one extreme to the other. This exercise reveals six areas for possible placement of aerosol channels. In these areas there are practically no effects from varying either ozone or water vapour optical depths, as it is emphasized in Figure 4 where the difference in transmittance for extreme cases is demonstrated. Each area houses one channel, except area ①, which uses two channels due to its large spectral width.

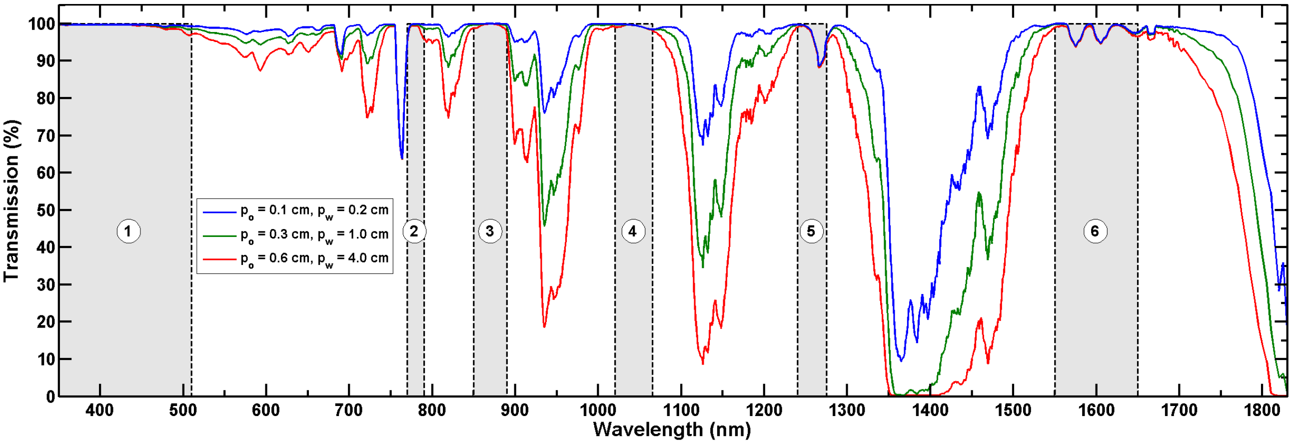

Figure 3. DNI beam transmittance without $\tau_{\mathrm{a}}(\lambda)$ and $\tau_{\mathrm{R}}(\lambda)$.

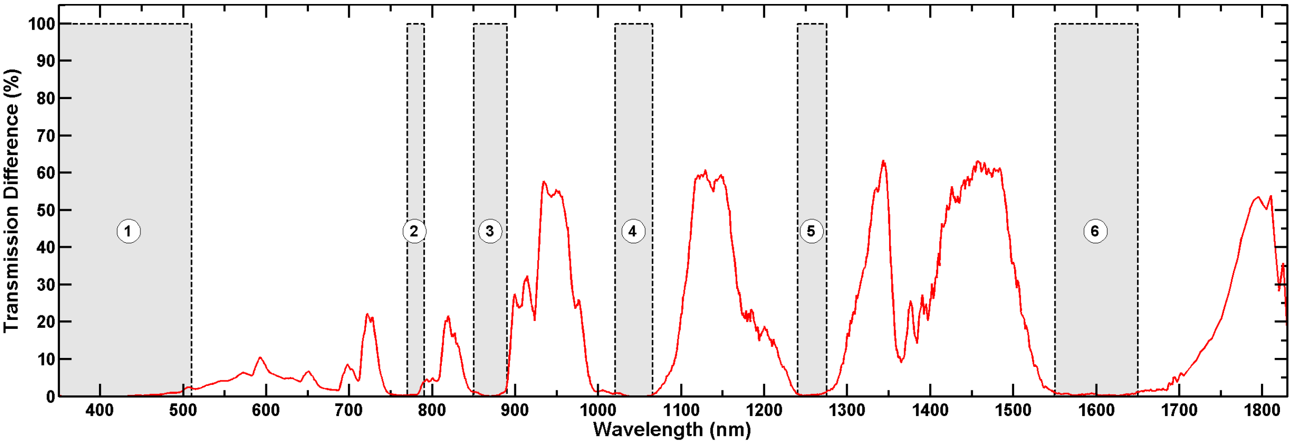

Figure 4. Difference in DNI beam transmittances without $\tau_{\mathrm{a}}(\lambda)$ and $\tau_{\mathrm{R}}(\lambda)$ for extreme cases.

The ozone absorption of the solar spectrum is very weak across the 350–1830 nm range, even under the most extreme of conditions, as shown in Figure 5. The region from 500–700 nm, also know as the Chappuis band, where the maximum ozone absorption occurs, is used to study the most suitable area for ozone channel placement. This point roughly corresponds to 600 nm. However, the inset plot in Figure 6 reveals moderate water vapour absorption for the 580–605 nm range. Therefore, the ozone channel is placed at 610 nm, which does not overlap with water vapour absorption but is still close to the peak ozone absorption.

The water vapour channel is also placed where its maximum absorption occurs. Suitable areas for a water vapour channel in the 350–1830 nm range are marked in Figure 6. Out of the 3 spectral bands, area ② is the most ideal, as it is more sensitive to water vapour absorption than area ①, yet it contains more incident power than area ③.

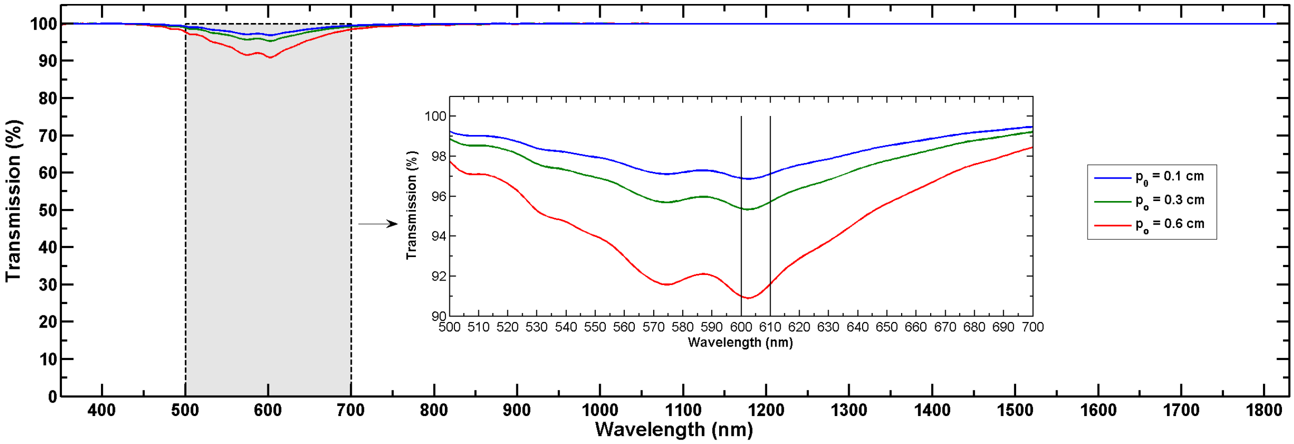

Figure 5. Ozone transmittance with varying pathlenghts.

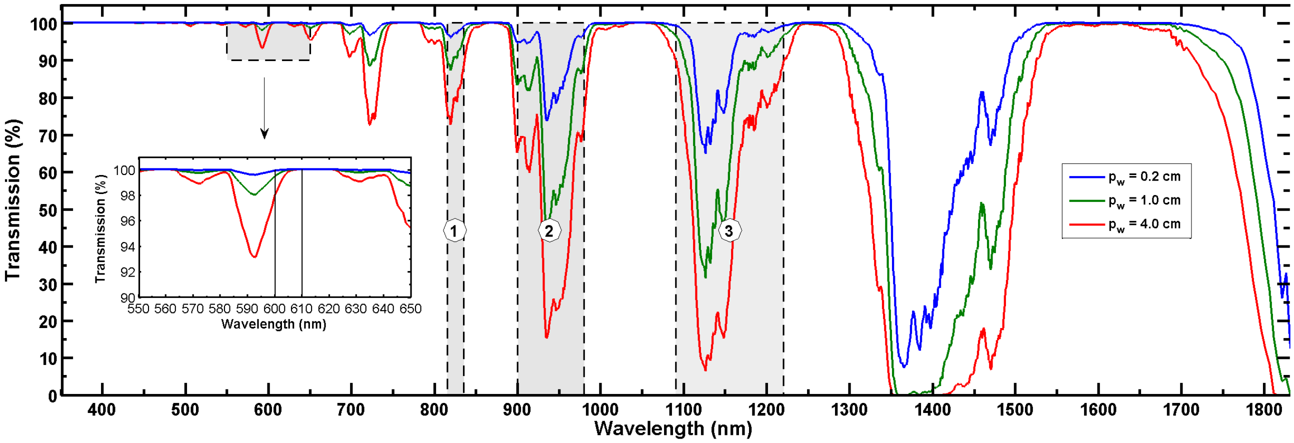

Figure 6. Water vapour transmittance with varying pathlenghts.

Table 3 summarizes channels and corresponding filter characteristics that are used in the simulation.

Table 3. MCFR's channels and filter characteristics.

Channel center (nm)	Parameter	FWHM (nm)	Max. transmittance (%)
420, 500, 780, 870, 1050, 1250, 1650	Aerosols	10	50
610	Ozone	10	50
940	Water vapour	10	50

2.4. Solar spectrum parameterization

The solar spectrum in (1) is obtained by determining the unknowns $T_{\mathrm{a}}(\lambda)$, $T_{\mathrm{o}}(\lambda)$, and $T_{\mathrm{w}}(\lambda)$. To derive these quantities, MCFR channels must be selected to isolate the effect of one atmospheric constituent at a time. This is accomplished by placing appropriate channels in the regions where only one unknown atmospheric parameter dominates. Figure 3 reveals areas that are unaffected by ozone and water vapour absorption. Channels in these regions are used to determine aerosol extinction. For example, channels centred at 500 nm and 780 nm (areas ① and ②, respectively, in Figure 3) can be used to deduce aerosol extinction for every wavelength in that range. Since the FWHM of each filter is 10 nm, the filter transmittance does not extend far from the centre wavelength. Hence, ozone and water vapour absorption can be neglected within the aerosol channels given in Table 3. The expression for the spectral irradiance of the aerosol channel centred at λ_{c} resembles (1) except that $T_{\mathrm{o}}(\lambda)$ and

$T_\mathrm{w}(\lambda)$ are set to unity for $\lambda_1 \leq \lambda \leq \lambda_2$, where $\lambda_1 = \lambda_\mathrm{c} - 25$ nm and $\lambda_2 = \lambda_\mathrm{c} + 25$ nm. Transmittance outside the given range is assumed to be negligible. Therefore, the simulated current of the photodiode for aerosol channel x can be expressed as

$$I_{x,\mathrm{simulated}} = A \cdot r^2 \cdot \int_{\lambda_1}^{\lambda_2} T_\mathrm{a}(\lambda) \cdot C_x(\lambda) \cdot d\lambda, \tag{11}$$

where $C_x(\lambda) = S_0(\lambda) \cdot T_\mathrm{g}(\lambda) \cdot T_\mathrm{n}(\lambda) \cdot T_\mathrm{R}(\lambda) \cdot F_x(\lambda) \cdot R(\lambda)$. The uniform trapezoidal rule is used to approximate the result of the integration in (11). The only outstanding unknown is $T_\mathrm{a}(\lambda)$, which can be expressed through a combination of Beer's and Ångström's power laws as

$$T_\mathrm{a}(\lambda) = \exp\big[- \beta_\mathrm{y} \cdot \mathrm{pow}(\lambda, -\alpha_\mathrm{y}) \cdot m_\mathrm{a} \big]. \tag{12}$$

For a given aerosol extinction region y, the values of α_y and β_y are optimized such that the simulated current of the photodiode from (11) agrees with the measured current from (10). In other words, the total residual difference between the simulated and measured current values is minimized for two channels that define the aerosol region. A 1-D Golden section search algorithm is used to find the values of α_y that produces the smallest residual error for 40 pre-defined values of β_y. Finally, the optimal values of α_y and β_y are passed to a 2-D simplex algorithm to further refine these parameters. This optimization routine is performed for each aerosol region y in order to determine the aerosol transmittance $T_\mathrm{a}(\lambda)$. Calculation of the aerosol transmittance is a crucial step in deriving ozone and water vapour column amounts.

The spectral irradiance for ozone and water vapour channels is very similar to (1), but $T_\mathrm{w}(\lambda)$ and $T_\mathrm{o}(\lambda)$ are set to unity, respectively. The simulated current of the photodiodes for these channels resembles (11) with the addition of the appropriate $T_\mathrm{o}(\lambda)$ or $T_\mathrm{w}(\lambda)$ term. The unknown ozone and water vapour transmittances are expressed through Beer's law in a similar manner to (12) with suitable formulations for optical depth and air mass. Both the ozone and water vapour total column abundances, p_o and p_w, are found with a 1-D Golden section search algorithm that minimizes the residual difference between simulated and measured current values. Once the parameterization is complete, the simulated spectral irradiance $S(\lambda)$ from (1) is computed and compared with the measured spectral irradiance from the FSR.

3. RESULTS

An extensive analysis spanning two years for 46,454 measured spectra from the University of Ottawa's CPV testing facility is performed to validate the developed algorithm for solar spectrum reconstruction. All spectra contain at least 200 W/m^2 of incident power in the measured 350–1830 nm range. The large number of spectra permits testing of the algorithm under a wide range of atmospheric inputs to ensure it is applicable to other locations with different climatic conditions. For example, Figures 7 and 8 show a six channel MCFR reconstruction that consists of four aerosol channels (420, 500, 780, and 1050 nm), the ozone channel (610 nm), and the water vapour channel (940 nm) under clear and hazy conditions in Ottawa. There is a high contrast in aerosol and water vapour content between both cases, yet the spectral reconstruction in each instance is accurate. This observation is emphasized by the inset plots in both figures that show in detail the effective simulation of water vapour absorption. Furthermore, in both cases, the total incident power between measured and simulated spectra are in excellent agreement. The total power difference is -6.1 W/m^2 (or -1.24 %) and -4.3 W/m^2 (or -0.5 %) for clear and hazy conditions, respectively. It must be noted that smoothing by central moving average is performed on the simulated spectrum to match its resolution with the measured spectrum.

Since it is not practical to analyze every spectrum in such detail manually, yearly simulations are performed. The RMS error and mean difference of the analyzed data sets with respect to the original measured spectra are calculated, as shown in Figures 9 and 10. This technique allows comparison of different channel configurations with ease. The lowest RMS error and mean difference typically occur in areas where the aerosol, ozone, or water vapour channels are located. The mean difference is calculated based on a weighted technique to avoid large differences between small irradiance values. The largest discrepancies occur at the very sharp and narrow oxygen absorption bands around 687 nm and 761 nm, because the FSR averages spectra with its spectral resolution over several nanometres. Overall, excellent agreement is demonstrated between measured and simulated spectra.

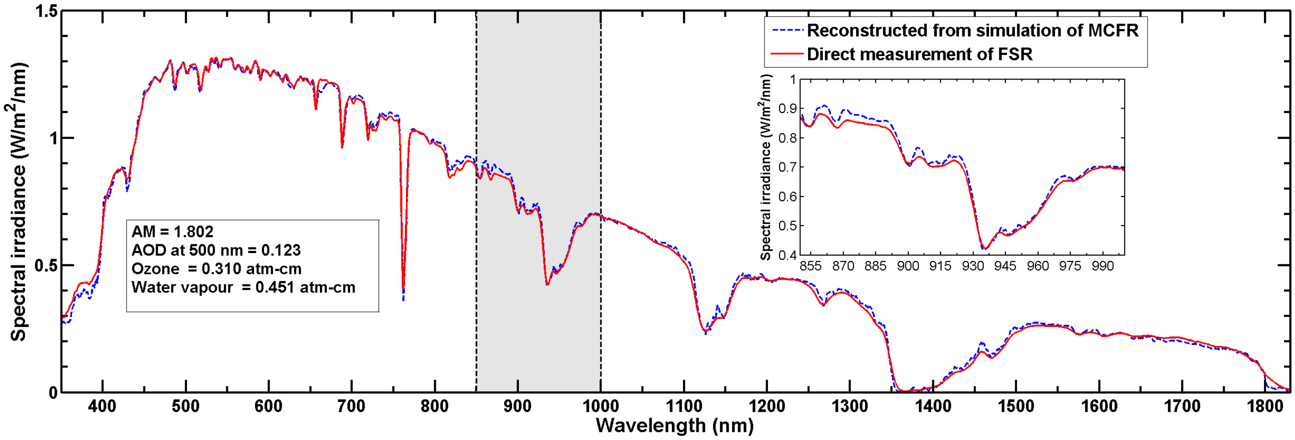

Figure 7. MFCR with 4 aerosol channels (420, 500, 780, and 1050 nm), ozone channel (610 nm) and water vapour channel (940 nm) under clear conditions in Ottawa.

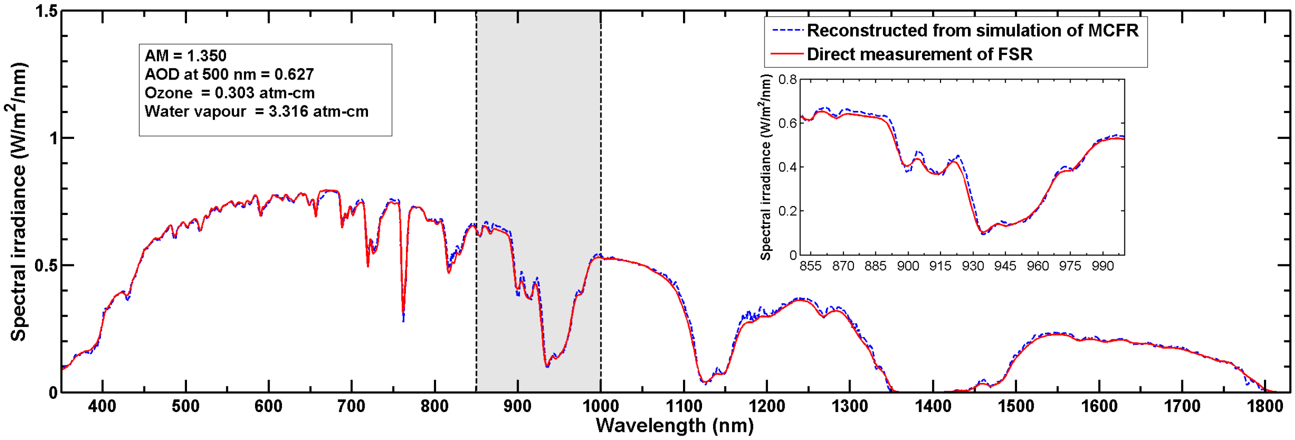

Figure 8. MFCR with 4 aerosol channels (420, 500, 780, and 1050 nm), ozone channel (610 nm) and water vapour channel (940 nm) under hazy conditions in Ottawa.

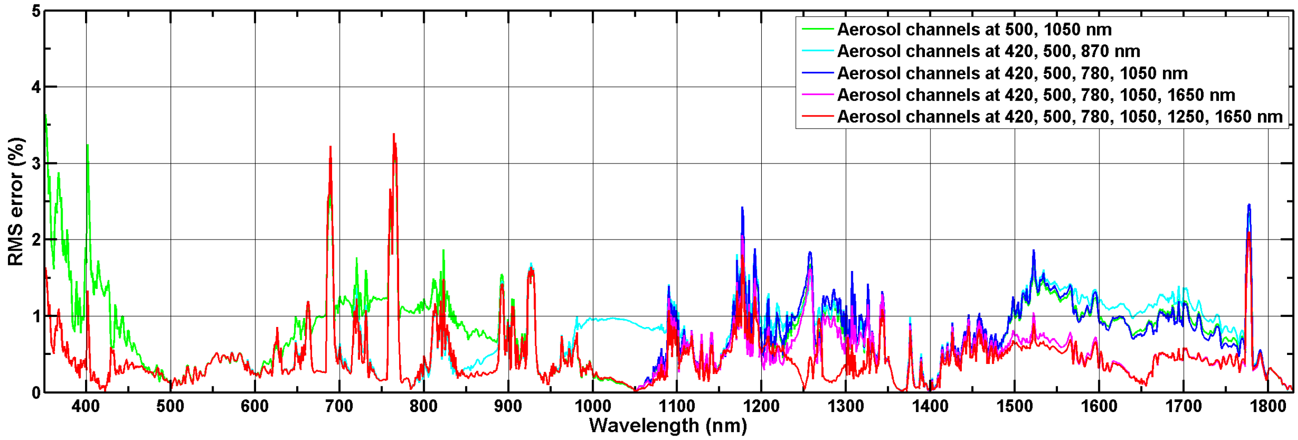

Figure 9. RMS error of reconstruction with respect to the input spectra for two to six aerosol channel MCFR for 2012 with 26,768 analyzed spectra.

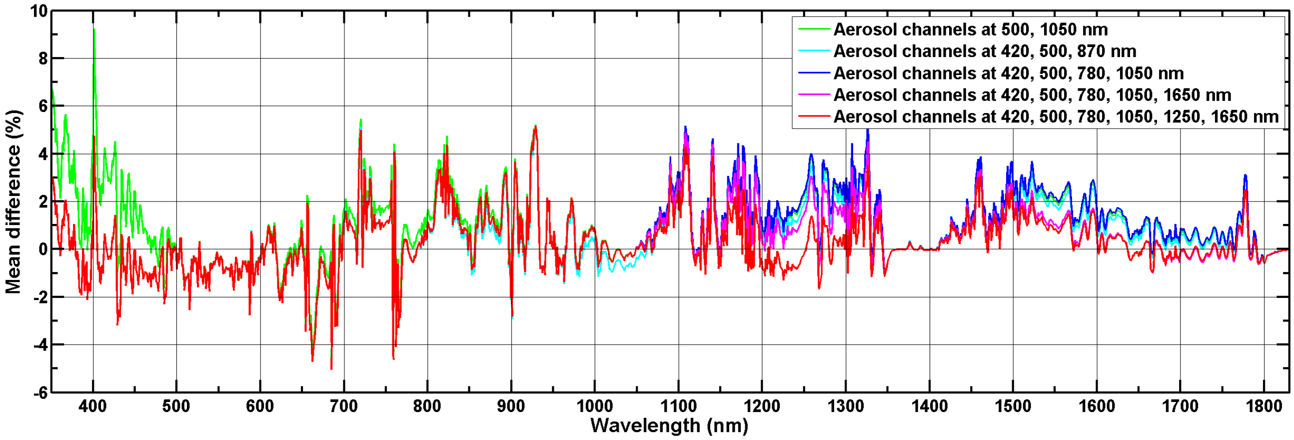

Figure 10. Mean difference with respect to the input spectra for 2 to 6 aerosol channel MCFR for 2012 with 26,768 analyzed spectra.

Table 4 summarizes the results of Figures 9 and 10 by highlighting the best aerosol channel combinations for a limited number of aerosol channels. For all of these cases, the ozone and water vapour channels at 610 nm and 940 nm, respectively, are included. To compare different aerosol channel combinations, the areas under the RMS error curves are normalized to the highest area or the worst performing configuration. The inverse of the resultant values is calculated to ensure that the worst performing channel combination has the lowest value. Table 4 reveals that the Ångström power law is not sufficient to estimate aerosol extinction across the entire measured spectral range. Application of the power law piece-wise, with different α_{y} and β_{y} parameters for each spectral range, gives more accurate fits to the measured data.

Table 4. Best aerosol channel combinations (2012 data set).

Aerosol channels	Best combination	Relative performance*
2	500, 1050 nm	1
3	420, 500, 870 nm	1.098
4	420, 500, 780, 1050 nm	1.271
5	420, 500, 780, 1050, 1650 nm	1.624
6	420, 500, 780, 1050, 1250, 1650 nm	1.796

Note: Relative performance is defined as the inverse of normalized area of the RMS error curve.

Although six aerosol channels give a very good spectral reconstruction accuracy, it is not generally desirable to have channels situated at 1250 and 1650 nm. These far infrared channels need expensive Ge or InGaAs detectors, which have bandgaps low enough to detect the irradiance at those wavelengths. On the other hand, Si-based detectors are relatively cheap and ubiquitous. Therefore, it is recommended to either use a three aerosol channel configuration of 420, 500, and 870 nm or a four channel configuration of 420, 500, 780, and 1050 nm. In both cases the standard deviation for the 2012 data set in Ottawa is under 1.5% over 96% of 350–1830 nm range.

4. CONCLUSION

The parameterization model for solar spectrum reconstruction with the simulated MFCR is described. The developed algorithm is applied to over 46,784 measured spectra from the University of Ottawa's CPV test facility to deduce the optimal combination of photodiode channels needed to extract the aerosol extinction, ozone and water vapour absorption. It is shown that for the entire data set of 2012 in Ottawa, the RMS error for Si-based MCFR with four aerosol channels (420, 500, 780, and 1050 nm), one ozone channel (610 nm), and one water vapour channel (940 nm) is under 1.5% over 96% of the 350–1830 nm range. Finally, it is revealed that the greater the number of aerosol channels, the better the reconstruction accuracy.

REFERENCES

[1] Chan, N., Brindley, H. E., and Ekins-Daukes, N. J., "Quantifying the impact of individual atmospheric parameters on CPV system power and energy yield," in [Photovoltaic Specialists Conference (PVSC), 2012 38th IEEE], 000922–000927, IEEE (2012).

[2] Chan, N., Young, T., Brindley, H., Ekins-Daukes, N. J., Araki, K., Kemmoku, Y., and Yamaguchi, M., "Validation of energy prediction method for a concentrator photovoltaic module in Toyohashi Japan," Progress in Photovoltaics: Research and Applications (2012).

[3] Jaus, J. and Gueymard, C. A., "Generalized spectral performance evaluation of multijunction solar cells using a multicore, parallelized version of SMARTS," in [AIP Conference Proceedings], 1477, 122 (2012).

[4] Chan, N., Young, T., Brindley, H., Chaudhuri, B., and Ekins-Daukes, N., "Variation in spectral irradiance and the consequences for multi-junction concentrator photovoltaic systems," in [Photovoltaic Specialists Conference (PVSC), 2010 35th IEEE], 003008–003012, IEEE (2010).

[5] Muller, M., Marion, B., Kurtz, S., and Rodriguez, J., "An investigation into spectral parameters as they impact CPV module performance," in [AIP Conference Proceedings], 1277, 307 (2010).

[6] Gueymard, C. A., "Daily spectral effects on concentrating PV solar cells as affected by realistic aerosol optical depth and other atmospheric conditions," in [SPIE Solar Energy and Technology], 741007–741007, International Society for Optics and Photonics (2009).

[7] Minemoto, T., Nagae, S., and Takakura, H., "Impact of spectral irradiance distribution and temperature on the outdoor performance of amorphous Si photovoltaic modules," Solar energy materials and solar cells 91(10), 919–923 (2007).

[8] Gottschalg, R., Betts, T., Infield, D., and Kearney, M., "The effect of spectral variations on the performance parameters of single and double junction amorphous silicon solar cells," Solar energy materials and solar cells 85(3), 415–428 (2005).

[9] Gottschalg, R., Infield, D., and Kearney, M., "Experimental study of variations of the solar spectrum of relevance to thin film solar cells," Solar energynergy materials and solar cells 79(4), 527–537 (2003).

[10] Gonzalez, M. and Carrol, J., "Solar cells efficiency variations with varying atmospheric conditions," Solar Energy 53(5), 395–402 (1994).

[11] King, R., Bhusari, D., Larrabee, D., and Liu, X., "Solar cell generations over 40% efficiency," Progress in Photovoltaics: Research and Applications 20, 801–815 (2012).

[12] ASTM, "G173-03: Standard tables for reference solar spectral irradiances: direct normal and hemispherical on 37° tilted surface," (2012).

[13] McMathon, W., Kurtz, S., Emery, K., and Young, M., "Criteria for the design of GalnP/GaAs/Ge triple junction cells to optimize their performance outdoors," National Renewable Energy Laboratory (2002).

[14] Al Taher, O., Cravens, R., Pien, P., Jones, R., Ermer, J., Hebert, P., and Chin, J., "Qualification testing of 40% metamorphic CPV solar cells," in [Photovoltaic Specialists Conference (PVSC), 2010 35th IEEE], 1995–1998, IEEE (2010).

[15] Gueymard, C. A., SMARTS2: a simple model of the atmospheric radiative transfer of sunshine (1995).

[16] Gueymard, C. A., "Parameterized transmittance model for direct beam and circumsolar spectral irradiance," Solar Energy 71, 325–346 (2001).

[17] Holben, B., Eck, T., Slutsker, I., and Tanre, D., "AERONET - A federated instrument network and data archive for aerosol characterization," Remote Sensing of Environment 66(1), 1–16 (1998).

[18] Holben, B., Tanre, D., Smirnov, A., and Eck, T., "An emerging ground-based aerosol climatology: Aerosol optical depth from AERONET," Journal of Geophysical Research: Atmospheres 106(D11), 12067–12097 (2001).

[19] Seckmeyer, G., Bais, A., Bernhard, G., Blumthaler, M., Johnsen, B., Lantz, K., and McKenzie, R., "Instruments to measure solar ultraviolet radiation, Part 3: Multi-channel filter instruments," World Meteorological Organization Global Atmosphere Watch, (2010).

[20] Reda, I. and Andreas, A., "Solar position algorithm for solar radiation applications," Solar energy 76(5), 577–589 (2004).

[21] Gueymard, C. A., "SMARTS code, version 2.9.5, user's manual," Solar Consulting Services (2006).

[22] Ångström, A., "On the atmospheric transmission of sun radiation and on dust in the air," Geografiska Annaler 11, 156–166 (1929).

[23] Jacobson, M. Z., [Fundamentals of atmospheric modeling], Cambridge University Press, New York, USA (2005).

[24] Gilbert, N. L., Goldberg, M. S., Beckerman, B., Brook, J. R., and Jerrett, M., "Assessing spatial variability of ambient nitrogen dioxide in Montreal, Canada, with a land-use regression model," Journal of the Air & Waste Management Association 55(8), 1059–1063 (2005).

[25] Bucholtz, A., "Rayleigh-scattering calculations for the terrestrial atmosphere," Applied Optics 34(15), 2765–2773 (1995).

[26] Bodhaine, B. A., Wood, N. B., Button, E. G., and Slusser, J. R., "On Rayleigh optical depth calculations," Journal of Atmospheric and Oceanic Technology 16, 1854–1861 (1999).